Dalton Transactions

PAPER

View Article Online
View Journal | View Issue

Cite this: *Dalton Trans.*, 2019, **48**, 12279

Positive shift in corrole redox potentials leveraged by modest β-CF_3-substitution helps achieve efficient photocatalytic C–H bond functionalization by group 13 complexes†‡

Xuan Zhan, [a] Pinky Yadav,[a] Yael Diskin-Posner, [b] Natalia Fridman,[a] Mahesh Sundararajan,[c,d] Zakir Ullah,[c,d] Qiu-Cheng Chen,[a] Linda J. W. Shimon, [b] Atif Mahammed,[a] David G. Churchill, *[a,c,d] Mu-Hyun Baik *[c,d] and Zeev Gross *[a]

Tris- and tetrakis-β-trifluoromethylated gallium (**3CF_3-Ga**, **4CF_3-Ga**) and aluminum (**3CF_3-Al**, **4CF_3-Al**) corrole systems were synthesized by a facile "one-pot" approach from the respective tri- and tetra-iodo starting compounds using the $FSO_2CF_2CO_2Me$ reagent. The isolated 5,10,15-(tris-pentafluorophenyl) corrole-based compounds set the groundwork for another important β-substituent study in inorganic photocatalysis. As seen previously, $-CF_3$ group substitution leads to red shifts in both the absorption and emission spectra compared to their unsubstituted counterparts (X. Zhan, *et al.*, *Inorg. Chem.*, 2019, **58**, 6184–6198). All CF_3-substituted corrole complexes showed strong fluorescence; **3CF_3-Al** possessed the highest fluorescence quantum yield (0.71) among these compounds. The photocatalytic production of bromophenol by way of these photosensitizing complexes was studied demonstrating that tris-trifluoromethylation is an important substitution class, especially when Ga^{3+} is present (experimental TON value in parentheses): **3CF_3-Ga** (192) > **4CF_3-Ga** (146) > **3CF_3-Al** (130) > **4CF_3-Al** (56) > **1-Ga** (43) > **1-Al** (18). The catalytic performance (turn-over number, TON) for benzylbromide formation (from toluene) was found to be: **3CF_3-Ga** (225) > **1-Ga** (138) > **3CF_3-Al** (130) > **4CF_3-Ga** (126) > **1-Al** (95) > **4CF_3-Al** (89); in these trials, benzaldehyde was also detected as a product in which **3CF_3-Ga** outperforms the other compounds (TON = 109). The tetra-CF_3-substituted **4CF_3-Ga** and **4CF_3-Al** species exhibit a dramatic formal positive shift of 116 mV and 126 mV per [CF_3] group, respectively, compared to the unsubstituted parent species **1-Ga** and **1-Al**. However, the absorbance values (λ_{abs} = 400 nm) of these corrole complexes (all equally concentrated: 4.0×10^{-6} M) were **3CF_3-Al** (0.23) > **3CF_3-Ga** (0.22) > **1-Al** (0.21) > **1-Ga** (0.20) > **4CF_3-Al** (0.19) > **4CF_3-Ga** (0.15), which helps rationalize why **3CF_3-Ga** performs the best among these catalysts. These new photosensitizers were carefully characterized by ^{1}H and ^{19}F NMR spectroscopy to help verify the number and position (symmetry) of the CF_3 groups; **3CF_3-Ga** and **3I-Al** were structurally characterized. Distortions in the corrole macrocycle imposed by the multiple β-substitution were quantified.

Received 22nd May 2019,
Accepted 16th July 2019

DOI: 10.1039/c9dt02150g

rsc.li/dalton

Introduction

Photosensitization in small molecules almost always requires a π-delocalized chromophoric system; its catalytic activity corresponds with the light energy provided, as well as conditions and the solvent environment, *etc*. Since the tuning of the aromatic π-system is best when it is rigid, effectively planar, structurally sound (robust), bioinspired, as well as easily functionalized, porphyrinoid systems of various types continue to be employed and interrogated as much as ever.[1] Recent photocatalysis articles dealing with C–H bond functionalization include studies in which C–H bonds can be oxidized and halogenated, *etc*.[1]

[a]*Schulich Faculty of Chemistry, Technion-Israel Institute of Technology, Haifa 32000, Israel. E-mail: ch10zg@technion.ac.il*
[b]*Department of Chemical Research Support, Weizmann Institute of Science, Rehovot 76100, Israel*
[c]*Department of Chemistry, Korea Advanced Institute of Science and Technology (KAIST), Daejeon, Republic of Korea. E-mail: david.churchill.korea@gmail.com*
[d]*Center for Catalytic Hydrocarbon Functionalizations, Institute for Basic Science (IBS), Daejeon, Republic of Korea*

†Dedicated to O. T. Beachley Jr. (1937–2018) a longtime faculty member at the University at Buffalo and specialist in main group chemistry.

‡Electronic supplementary information (ESI) available: Details of all the experimental data and all spectra of characterization. CCDC 1868043 and 1915746. For ESI and crystallographic data in CIF or other electronic format see DOI: 10.1039/c9dt02150g

In chromophores as well as medicinal compounds, fluorine substituent chemistry continues to develop very rapidly.[2] An estimated 30% of modern molecular pharmaceuticals contain at least one fluorine atom; this substitution enhances lipophilicity and membrane permeability.[3] Therefore, with sterics roughly of an H-atom, but with great polarization capacity, the preferred tweaking of the electronics and other molecular properties has, in many cases, been realized. $-CF_3$ groups possess extraordinary Hammett parameter values (σ_m = 0.43; σ_p = 0.54).[4] The F group is stable, chemically compatible, and biocompatible.[5] Incorporation of such chemical groups in the form of trifluoromethylation is also straight-forward and paves the way for the preparation of natural or synthetic (medicinal) fluoroorganic/fluoroorganometallic derivatives.[6] While there have been a variety of synthetic approaches to corrole β-position substitution chemistry, those bearing both bare fluorines, as well as CF_3 groups, prove especially intriguing in the context of photosensitizer design. Recent publications have addressed the utility of $-CF_3$-containing corroles[7] which, as with the original synthetic issue that lead to the widespread use of the *meso*-C_6F_5 substituents, also revolves around achieving practical synthetic methodology. Structure–function relationships in the context of photocatalysis can be elucidated from the corrole system's reliable functional group layout and its tunable and optimizable properties.[7]

Perfluoroalkyl-substituted corroles and their metallic complexes have shown their robust potential in energy-related catalysis, organic catalysis, and medicinal chemistry utility.[8] In 2008, Ghosh and coworkers reported on the copper β-octakis (trifluoromethyl) corroles, and later, on the *meso*-CF_3 substituted free-base corrole and its cobalt complex.[9] Recently, we reported the halogenation on the β-position of 5,10,15-(tris-pentafluorophenyl)corrole (tpfc) which helped tune the redox and photophysical properties.[10] Recently, our group fruitfully achieved the synthesis of *meso*-5,10,15-tris-trifluoromethylated corrole (TFC) and its metal complexes.[11] In the meantime, we successfully prepared the partially β-CF_3 substituted gold corroles; a dramatic effect of CF_3-substitution is imparted to the photophysical and redox properties of the system.[12] Therefore, papers dealing with CF_3 group corroles, while still rare, are already starting to redefine the photocatalytic research front.[7] Unlike the gold corrole, which was non-fluorescent, and different in many ways from P chemistry, we can adapt intriguing photophysical features observed in examples of corroles featuring main group elements as the central atom; therefore, β-CF_3 substitution could help *turn on* C–H bond activation chemistry when considering the β-unsubstituted aluminium (**1-Al**) and gallium (1-Ga) species. Thus, we set out to prepare partially β-trifluoromethylated aluminium and gallium complexes to obtain deeper insights into the effect of CF_3-substitution on photophysical and electrochemical redox properties. With the issue of C–H bond activation at hand, we turned to the literature where Gryko and co-workers reported that porphyrins can be used as photocatalysts in, *e.g.*, C–C bond formation reactions and C–E activation reactions;[13] this aroused great interest to investigate whether examples of corrole complexes can be found that signify promising precursors/candidates for photo-synthesis applications. Thus, the potential of these newly synthesized non-precious element containing corroles was addressed using light energy; readily available HBr is employed to achieve an understanding of the patterns of organic substrate functionalization.

Results and discussion

Scheme 1 depicts the synthetic method for the preparation of the target compounds under discussion. The synthesis of precursors (**3I-Ga**, **4I-Ga**, **3I-Al**, **4I-Al**) have been described previously.[14] The treatment of the appropriately iodinated metallocorroles with methyl-2,2-difluoro-2-(fluorosulfonyl)acetate ($FSO_2CF_2CO_2Me$) and CuI in DMF at 100 °C under argon atmosphere yielded colored β-CF_3-substituted target compounds in 42–53% yield. All iodo positions were logically exchanged for $-CF_3$ groups, as expected. All new metallocorroles were characterized by various spectroscopic techniques *viz.*, NMR spectroscopy (complete versions of spectra see Fig. S1–S8‡), MS (see Fig. S9–S14‡) and UV-vis. Through the NMR spectroscopic studies, **3CF$_3$-Ga** and **3CF$_3$-Al** were found to exhibit singlets at 9.43 and 9.27 ppm, respectively; whereas two doublets of **4CF$_3$-Ga** (8.30 ppm and 8.13 ppm) and **4CF$_3$-Al** (8.10 ppm and 7.91 ppm) corresponding to β-pyrrole protons were found upfield shifted. The greater number of CF_3-substitutents resulted in higher symmetry of the macrocycle and fewer signals, and signals which are again drawn upfield (Fig. 1a). Spectroscopic characterization was extended to ^{19}F NMR spectroscopy and confirming the assignments of the symmetric tetrasubstituted species made by ^1H NMR spectroscopy: three *para*-F resonance signals showed 1 : 2 integration ratio rather than a 2 : 1 or 1 : 1 : 1 ratio (observed in **3CF$_3$-Al** and **3CF$_3$-Ga**) (Fig. 1b). These spectroscopic results matched the number of groups and extent of molecular symmetry exhibited and reflects that expected for the molecular structures.

Experimental conditions were found for compounds **3CF$_3$-Ga** and **3I-Al** as to enable them to crystallize out of solution reasonably well. X-ray quality crystals of **3CF$_3$-Ga** were therefore obtained by slow evaporation from ethanol/hexane solution.

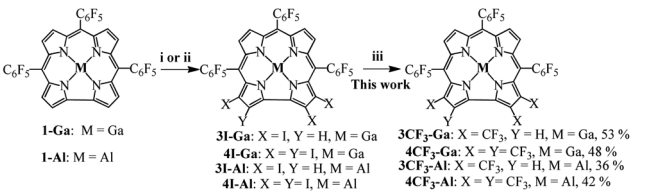

Scheme 1 The synthetic route of target compounds: **3CF$_3$-Ga**, **3CF$_3$-Al**, **4CF$_3$-Ga** and **4CF$_3$-Al**. All axial ligands of these compounds have been omitted for clarity. Synthetic methods i and ii have been reported previously and their procedures can be found in the published literature.[14] (i) An excess stoichiometric amount of NIS (*N*-iodosuccinimide) was added in acetonitrile at room temperature for 1 h to give **4I-Ga**/**4I-Al**; (ii) treatment with excess I_2 and pyridine and refluxing in toluene for 1 h gives **3I-Ga**/**3I-Al**; (iii) $FSO_2CF_2CO_2Me$/CuI, DMF, 100 °C, 10 h.

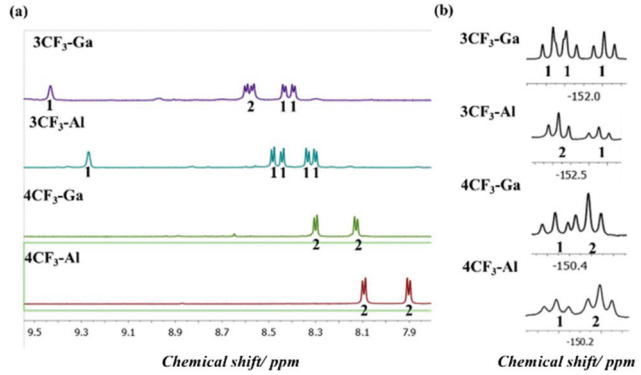

Fig. 1 (a) ^{1}H NMR spectra ($CDCl_3$, 400 MHz) of the available β-pyrrole CH's for **3CF$_3$-Ga**, **3CF$_3$-Al** and **4CF$_3$-Ga**, **4CF$_3$-Al** were recorded in C_6D_6; (b) their corresponding partial ^{19}F NMR spectra ($CDCl_3$, 377 MHz), focusing on *para*-F [$-C_6F_5$] atoms only.

X-ray quality crystals of **3I-Al** were obtained by slow evaporation of chloroform/hexane solution with an addition of a few drops of pyridine to provide the central metal sites access to a coordinating solvent species. The structure of **3CF$_3$-Ga** was confirmed by X-ray crystallography. Interestingly, in this complex, we found the gallium metal centre was not only coordinated to the N-atoms from four pyrrole units but also bound to a solvent molecule that refined well as a water molecule; the single axial ligand assigned structurally as a [H_2O] unit allowed the metal complex to adopt a domed conformation (Fig. 2); the Ga–O bond length was observed to be 1.870(4) Å. As expected from the electronic effect of the β-substituted iodine, the average Al–$N_{pyrrole}$ bond length of **3I-Al** was found to be 1.899(5) Å which was slightly longer than the bond length found for **1-Al** (1.892(5) Å); whereas the average Al–$N_{pyridine}$ bond length of **3I-Al** (2.154(4) Å) was found to be somewhat shorter than that found in **1-Al** (2.183(8) Å). All selected structural data is shown in Table S1;‡ interestingly, the **3CF$_3$-Ga** species exhibited a more distorted macrocycle compared to the previous reported iodinated species **3I-Ga**:[1] the deviation of the central gallium from the [N_4] corrole plane

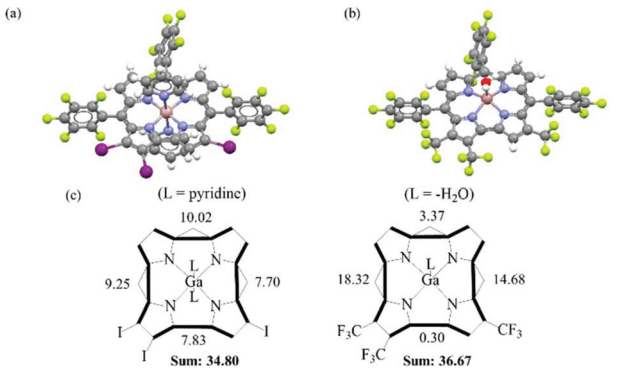

Fig. 2 Side views of the X-ray crystal structures of **3I-Al** (a) and **3CF$_3$-Ga** (b); (c) a comparison of the dihedral angles (°) and sum values found for **3I-Ga** and **3CF$_3$-Ga**.

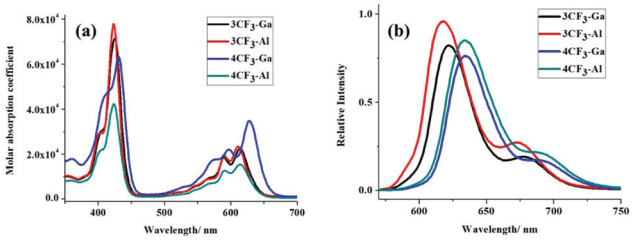

Fig. 3 (a) The UV-vis spectra of the investigated compounds: **3CF$_3$-Ga** (1.55×10^{-5} M), **3CF$_3$-Al** (1.34×10^{-5} M), **4CF$_3$-Ga** (1.65×10^{-5} M), **4CF$_3$-Al** (2.65×10^{-5} M). (b) The fluorescence emission spectra of studied compounds under the same absorbance (0.05 OD) with the Soret band of TPP also (5,10,15,20-tetraphenylporphyrin) recorded for comparison. All data recorded in toluene under room temperature and aerobic conditions were and the excitation wavelength was set at 420 nm.

(0.0232(6) Å) is somewhat greater than that found for **3I-Ga** (0.0182(4) Å). The dihedral "saddling" angles also demonstrated this notion: the sum values of four dihedral angles were determined as 34.80° (**3I-Ga**) *vs.* 36.67° (**3CF$_3$-Ga**).

We then undertook a full set of UV-vis and fluorescence studies of the corrole photosensitizer molecules. The UV-vis absorption (see Fig. 3a) spectral data of β-CF_3 substituted corroles are listed in Table S2.‡ The electron-withdrawing nature of the $-CF_3$ group attenuated the strength of the spectral absorption in the red region. Tetra-CF_3-substituted aluminium and gallium corroles displayed a small 5–6 nm shift in the Soret band maxima (centered around 420 nm); a more significant 19–27 nm shift was observed for the Q-band maxima, compared to the non-substituted **1-Al** and **1-Ga** species. All CF_3-substituted corrole complexes showed strong fluorescence; **3CF$_3$-Al** possessed the highest fluorescence quantum yield (Φ_F = 0.71) among these compounds. Interestingly, **4CF$_3$-Ga** showed a longer fluorescence lifetime (4.54 ns) than that for **1-Ga** (2.21 ns) and exhibited the largest non-radiative rate constant ($K_{nr} = 4.02 \times 10^8$ s^{-1}) (see Table S1‡) which can be explained by the "heavy atom effect" emanating from the gallium center, as well as by the effect of distortion from planarity based on the presence of the sterically congested CF_3 groups located at the 2, 3, 17 and 18 positions. The **3CF$_3$-Al** and **4CF$_3$-Al** showed stronger fluorescence than the **3CF$_3$-Ga** and **4CF$_3$-Ga** species. $-CF_3$ substitution also created the red shift in terms of the emission peak ranging from an increase in 12–17 nm as observed from the formal addition of a $-CF_3$ group onto **3CF$_3$-Ga**/**Al** to give **4CF$_3$-Ga**/**Al** (see Table S2‡).

To study the influence of CF_3-substitution on redox potentials of gallium and aluminium corroles, cyclic voltammetry (CV) experiments were obtained and the data was analysed (see Fig. 4, Fig. S15 and Table S3‡).

CV studies help elucidate the electronic effects of substituent incorporation as well as assess HOMO–LUMO levels. Several interesting points are noted here: (i) **4CF$_3$-Ga** and **4CF$_3$-Al** exhibited two reduction processes at −1.07 and −1.64 V; −1.11 and −1.59 V, respectively (see Fig. S15 and Table S3‡). (ii) Generally, with the same β-functionalization, the Ga corrole shows a more positive shift in redox potentials compared to

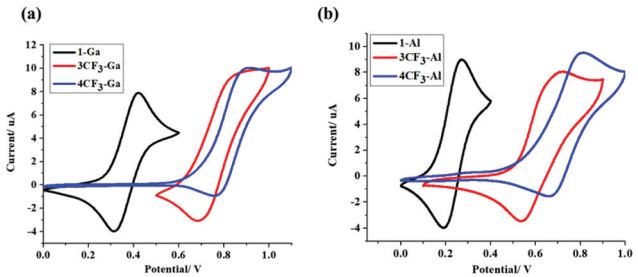

Fig. 4 (a) CV traces of **1-Ga**, **3CF$_3$-Ga** and **4CF$_3$-Ga** in the voltammogram region of compound oxidation. (b) CV traces of **1-Al**, **3CF$_3$-Al** and **4CF$_3$-Al** in the voltammogram region of compound oxidation. Glassy carbon working electrode, and an Ag/AgNO$_3$ ref. electrode. Solvent: CH$_3$CN with TBAP. Scan rate of 100 mV s^{-1} was applied.

the Al^{3+} corrole; however, notably, the 1st reduction potential for **3CF$_3$-Al** (−1.24 V) experienced a more positive shift than that for **3CF$_3$-Ga** (−1.26 V). (iii) The oxidation potential values observed for CF$_3$-substituted Ga/Al corroles is found to be below 1.0 V; **4CF$_3$-Ga** showed the most positive shift in oxidation potential located at 0.83 V. **4CF$_3$-Ga**/**Al** shifts the oxidation potential towards a more positive range by 116–126 mV per –CF$_3$ group compared to their unsubstituted counterparts (**1-Ga**/**1-Al**). The effect of the CF$_3$ group on redox potentials is more prominent than halogen substitution; Cl-substitution, for example, illustrates a formal maximum shift of 58 mV per group on the system.[14] Moving from 3CF$_3$ to 4CF$_3$-substitution, a greater positive shift in redox potentials was observed; 113 mV on the 1st oxidation potential and 187 mV shift on the 1st reduction potential for the same metal center shows the profound effect of the formal incorporation of a single extra –CF$_3$ group. (iv) The HOMO–LUMO energy gap decreased from 3CF$_3$ to 4CF$_3$ (2.02 V to 1.90 V for gallium complexes and from 1.87 V to 1.85 V for aluminium complexes). These findings remind us that trifluoromethylation is a good synthetic approach to help shift the redox potentials positive, and thus a tool to help reduce the HOMO–LUMO energy gap.

The dramatic positive shift in redox potentials of these newly CF$_3$-substituted gallium and aluminium corrole complexes, combined with their nature of photosensitization, inspired us to explore and develop their photocatalytic potential. The facile bromination of organic substrates is a research topic of significant interest due to its versatile (and potential emergent) applications in industrial and medicinal use; brominated (halogenated) organic compounds, especially aromatics, are versatile precursors for carbon–carbon and carbon–heteroatom bond formation such as the famous named cross-coupling reactions (*i.e.*, the illustrious Suzuki, Heck, Stille coupling reactions).[15] Specifically, we used phenol as a substrate and HBr as the bromide source along with the photosensitizer corrole photocatalyst taken under irradiation by a LED lamp (λ_{excit} = 395–405 nm, 200 W); different gallium and aluminium corroles were explored as catalysts to investigate the structure–function relationship of the catalysis (see additional operating information in the ESI‡). The reaction affords two mono-brominated phenol compounds (*ortho*- and *para*-, see Scheme 2, eqn (1)). All samples studied remained stable during the photocatalytic process as exemplified by a close comparison of the spectra *e.g.* for **3CF$_3$-Ga** (Fig. 5b) acquired before and after photocatalysis.

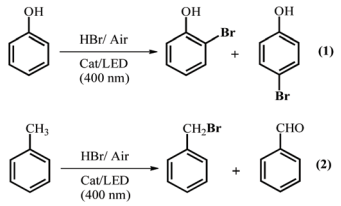

Scheme 2 Schemes for the photo-catalytic bromination of phenol and toluene under discussion here.

The corresponding results have been included and summarized in Table 1. Photocatalytic results obtained under the same conditions afforded turn-over number values (TON) of 43, 18, 192, 130, 146 and 56 for compounds **1-Ga**, **1-Al**, **3CF$_3$-Ga**, **3CF$_3$-Al**, **4CF$_3$-Ga** and **4CF$_3$-Al**, respectively, when they were used as catalysts. The photocatalytic performance for photosynthesis of bromophenol of these complexes is **3CF$_3$-Ga** > **4CF$_3$-Ga** > **3CF$_3$-Al** > **4CF$_3$-Al** > **1-Ga** > **1-Al**, which is roughly in

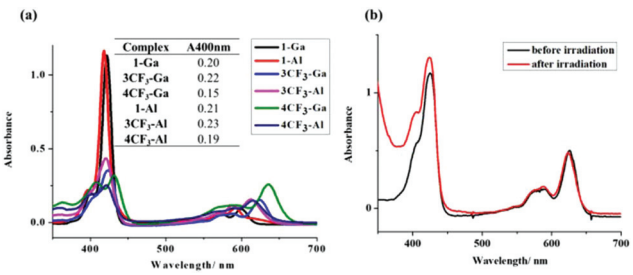

Fig. 5 (a) UV-vis spectra of investigated compounds under the same concentration of 4 × 10^{-6} M; inset: the table of the absorbance values at 400 nm; (b) UV-vis spectra of reaction mixture of **3CF$_3$-Ga** with HBr before and after 24 h of irradiation.

Table 1 Results from metallocorrole-catalyzed bromination of phenol giving both *ortho*-brominated and *para*-brominated phenol

Entry	Catalyst	Irradiation time (h)	λ_{max} of lamp (nm)	Bromo-phenol (TON)[a]
1	**1-Ga**	3	400	43
2	**1-Al**	3	400	18
3	**3CF$_3$-Ga**	3	400	192
4	**3CF$_3$-Ga**	3	595	30
5	**3CF$_3$-Al**	3	400	130
6	**4CF$_3$-Ga**	3	400	146
7	**4CF$_3$-Al**	3	400	59
8	No catalyst	3	400	—
9	**3CF$_3$-Ga**	3	Dark	—
10	**3CF$_3$-Ga**	12 (anaerobic)	400	—

[a] Turnover number of both *ortho*- and *para-mono*-brominated phenol formed as detected by GC (see ESI‡).

the order of the 1st oxidation potential values of these complexes: **4CF$_3$-Ga** (0.83 V) > **3CF$_3$-Ga** (0.77 V) > **4CF$_3$-Al** (0.74 V) > **3CF$_3$-Al** (0.62 V) > **1-Ga** (0.37 V) > **1-Al** (0.23 V), which confirmed that the complexes which possessed more positive redox potentials tended to have greater efficiency of photooxidation. The emitting light source here is the LED possessing a wavelength of *ca.* 400 nm; thus, under the same concentrations, the complexes which had stronger absorbance at 400 nm should perform more efficiently in photocatalysis.[16] The absorbance at the wavelength of 400 nm of these corrole complexes at exactly the same concentration (4×10^{-6} mol L^{-1}) was measured and found to be in the order of **3CF$_3$-Al** (0.23) > **3CF$_3$-Ga** (0.22) > **1-Al** (0.21) > **1-Ga** (0.20) > **4CF$_3$-Al** (0.19) > **4CF$_3$-Ga** (0.15) (Fig. 5(a)); the values help rationalize why **3CF$_3$-Ga** performed the best among these catalysts in the present study.

Halogenations of alkyl aromatics are very important and versatile reactions.[17] After successful trials of bromination of sp^2-C (phenol) herein, we further introduced this novel method for the photo-bromination of toluene (sp^3-C) to benzyl bromide (Table 2, entry 2). All new prepared aluminium and gallium corroles were investigated as the photocatalysts in driving this conversion. After irradiation for 5 hours under the LED (experimental details are provided in the ESI‡), the TON data was acquired; the results obtained by these metallocorroles have been included in Table 2. The catalytic performance (TON) for these catalysts was found to be: **3CF$_3$-Ga** (225) > **1-Ga** (138) > **3CF$_3$-Al** (130) > **4CF$_3$-Ga** (126) > **1-Al** (95) > **4CF$_3$-Al** (89). Besides benzyl bromide, benzaldehyde formation was also detected, determined to be a side-product involving smaller turnover efficiency. **3CF$_3$-Ga** outperforms others for the toluene-to-benzaldehyde conversion among these catalysts, with a TON of 109 for benzaldehyde and TON of 225 for benzyl bromide. The outstanding performance of **3CF$_3$-Ga** helped confirm and support our above explanation based on both absorbance and CV data. Considering the Q band absorption around 600 nm of studied corrole complexes, we wondered about the catalytic performance using the LED with irradiation wavelength at the Q band absorption; we adopted one LED (λ_{excit} = 595 nm, 200 W) as the irradiation source and took the best catalyst-**3CF$_3$-Ga** as an example, for conducting the phenol and toluene assays under the same concentration and irradiation time as before. The results were shown in Table 1 (entry 4) and Table 2 (entry 4); the turnover number (TON) of the photo-bromination of phenol and toluene were determined to be 30 and 24, respectively, which suggesting the much worse catalytic efficiency compared to assays using the higher energy LED (λ_{excit} = 395–405 nm, 200 W). The observed reduced product yields under *red* light irradiation (λ_{excit} = 595 nm, 200 W) using the most active photocatalysts herein was not surprising; the absence of benzaldehyde as a product suggests that the oxygen-involved catalytic reaction system was poorly triggered under red light irradiation. Benzaldehyde may form, but in amounts too miniscule to be detected by GC. Detailing the accessibility of the different possible photolytic pathways under different light sources will be an important objective in future studies. Clearly, under red light irradiation the major reaction is still at play: photooxidation of Br^- to form Br–Br which is then able to undergo reaction with the organic C(Ar)–H group.

The mechanism of conversion from bromide to bromine in the context of corrole research has been detailed in our previous work.[7,16] Additionally, the photocatalytic bromination mechanism of aromatics, as well as related oxygenation reactions have been investigated thoroughly by S. Fukuzumi and coworkers.[18] These authors suggested that the aromatic molecule would take the form of a radical cation and undergo reaction with Br^- to produce the radical adduct which would then be dehydrogenated by $HO_2^{\bullet}$ to generate brominated products; on the other hand, the radical cation could undergo deprotonation and be followed by fast oxygen addition and finally disproportionation to form the corresponding aldehyde. The formation of H_2O_2 here serves as support for the superoxide anion mechanism; H_2O_2 was detected indeed, *via* the I^-/I_3^- titration method monitored by UV[19] in one reaction mixture (when using **3CF$_3$-Ga** as a catalyst for the bromination of phenol) after irradiation (ESI‡). After adding excess TBAI (tetrabutylammonium iodide), the UV-vis spectrum showed typical absorption peaks of I_3^- in acetonitrile (Fig. S16‡).

Table 2 Metallocorrole-catalyzed bromination of toluene giving both products of benzyl bromide and benzaldehyde

Entry	Catalyst	Irradiation time (h)	λ of lamp (nm)	Benzyl bromide (TON)[a]	Benzaldehyde (TON)[b]
1	**1-Ga**	5	400	138	46
2	**1-Al**	5	400	95	42
3	**3CF$_3$-Ga**	5	400	225	109
4	**3CF$_3$-Ga**	5	595	24	—
5	**3CF$_3$-Al**	5	400	130	49
6	**4CF$_3$-Ga**	5	400	126	50
7	**4CF$_3$-Al**	5	400	89	30
8	No catalyst	5	400	—	—
9	**3CF$_3$-Ga**	5	Dark	—	—
10	**3CF$_3$-Ga**	24 (anaerobic)	400	—	—

[a] Turnover number of benzyl bromide as detected by GC (See ESI‡). [b] Turnover number of benzaldehyde detected by GC.

Conclusions

We have successfully prepared tris- and tetra-β-CF$_3$-substituted gallium and aluminium tpfc from the corresponding iodo-containing precursors. These novel products were prepared in sufficient yield in "one pot"; compound purity *via* excellent chromatographic separation allowed for the study of important substituent effects in photocatalytic studies. For a first measure, –CF$_3$ group substitution leads to red shifts in the absorption and emission spectra compared to their unsubstituted counterparts. By way of CV, the tetra-CF$_3$-substituted **4CF$_3$-Ga** and **4CF$_3$-Al** exhibit a dramatic positive shift of 116 mV and 126 mV, respectively, per –CF$_3$ group present

when compared to the completely β-unsubstituted parent species **1-Ga** and **1-Al**. While the NMR spectroscopic characterization of the four compounds helps generate a nice comparison graphically due to the obtained spectra, the trisubstituted version with gallium, with three groups instead of four, was found to be the top performer! The absorbance of these corrole complexes under the same concentration of 4×10^{-6} mol L^{-1} were determined to be in the order of **3CF$_3$-Al** (0.23) > **3CF$_3$-Ga** (0.22) > **1-Al** (0.21) > **1-Ga** (0.20) > **4CF$_3$-Al** (0.19) > **4CF$_3$-Ga** (0.15) (Fig. 5a), which served to help rationalize why the aforementioned **3CF$_3$-Ga** performed the best among these catalysts under the given conditions. Importantly, more than a 100 mV positive shift per $-CF_3$ was determined, compared to the fully unsubstituted species **1-Ga** and **1-Al**. This trifluoromethylation approach rendered the corrole complexes more efficient as photocatalysts in driving the photobromination of aromatic compounds here, as exemplified by phenol and toluene as starting materials. The general findings for the photocatalysis are from phenol to 2- or 4-bromophenol; the compound **3CF$_3$-Ga** (TON = 192) was much more active over the non-functionalized species **1-Ga** and **1-Al**. For benzyl bromide, **3CF$_3$-Ga** (TON = 225) dominated. Benzaldehyde was also detected with a relatively smaller turnover efficiency; it is a side product due to a separate reaction. Also, it is found to be highest when **3CF$_3$-Ga** is used. These photosensitizing compounds were isolated and carefully characterized by ^{1}H and ^{19}F NMR spectroscopy to determine the number and positioning of the CF_3 groups, which involved interpreting not only the extent of shifting of the signals, but also the degree of symmetry that the signals are revealing. Characterization also involved single-crystal characterization for **3CF$_3$-Ga**. The multiple trifluoromethylation groups induce distortions on the corrole macrocycle as judged by X-ray structural comparisons. As seen in previous studies, these deformations induced differences in redox properties and can contribute to differences in photocatalysis. Therefore, their photophysical and redox properties of **3CF$_3$-Al**, **4CF$_3$-Al**, **3CF$_3$-Ga**, **4CF$_3$-Ga** were clearly delineated. Our work is helpful for researchers seeking future designs of corroles: those wanting to (i) develop new classes of non-precious metal containing photocatalysts/photosensitizers and (ii) those seeking to unlock inherent photocatalysis in uninitiated systems.

Experimental

See the ESI‡ for further (full) experimental details.

Synthesis of 3CF$_3$-Ga

Dry portions of 3I-Ga (40 mg, 32 μmol) and CuI (0.19 g, 1 mmol) were dissolved in 5–10 mL DMF within 5 min under argon. Then, methyl-2,2-difluoro-2-(fluorosulfonyl) acetate ($FSO_2CF_2CO_2Me$) (0.13 mL, 1 mmol) was added into the reaction and the reaction flask was maintained at a temperature of 100 °C. After an ample time of 10 h, the reaction was monitored by TLC. After all starting materials were consumed, the reaction was stopped and the components were separated between water and CH_2Cl_2 (1 : 1 by volume) fractions; the organic phase was then evaporated. The greenish crude product was purified using silica gel chromatography with ethyl acetate and hexane (1 : 1 by volume) as the mobile phase. The fluorescent fraction was clear by inspection and collected/isolated; the involatile product was recrystallized using CH_2Cl_2 and hexane (1 : 1 by volume), to obtain a pure green solid portion of **3CF$_3$-Ga** obtained in a yield of 53% (17 mg). ^{1}H NMR (400 MHz, $CDCl_3$): δ = 9.43 (s, 1H), 8.59 (overlapping d, 2H), 8.42 (overlapping d, 2H), 7.34 (t, J_{H-H} = 7.56 Hz, 2H, pyridine-H), 6.78 (broad s, 4H, pyridine-H), 6.14 (broad s, 4H, pyridine-H). ^{19}F NMR (377 MHz, $CDCl_3$): δ = −48.88 (q, J_{F-F} = 12.05 Hz, 3F), −50.52 (q, J_{F-F} = 11.98 Hz, 3F), −53.25 (s, 3F), −137.65 (q, J_{F-F} = 9.30 Hz, 4F, *ortho*-F), −138.03 (m, 2F, *ortho*-F), −151.85 (q, J_{F-F} = 22.65 Hz, 2F, *para*-F), −152.08 (t, J_{F-F} = 21.90 Hz, *para*-F), −161.19 (m, 2F, *meta*-F), −162.85 (m, 4F, *meta*-F). MS^- (APCI, negative mode) for $C_{40}H_5F_{24}N_4Ga$: m/z = 1065.9381 (calculated), 1065.9297 (observed).

Synthesis of 4CF$_3$-Ga

A dry portion of 4I-Ga (40 mg, 30 μmol) and CuI (0.23 g, 1.2 mmol) were dissolved in 5–10 mL DMF after 5 min under argon. Then, methyl-2,2-difluoro-2-(fluorosulfonyl) acetate ($FSO_2CF_2CO_2Me$) (0.16 mL, 1.2 mmol) was added into the reaction solution and the temperature was maintained at 100 °C. The reaction was monitored by TLC. After an ample time of 10 h, the reaction was stopped, and the components were separated with water and CH_2Cl_2 (1 : 1 by volume); then the organic phase was evaporated. The crude product, which was green, was then purified using silica gel chromatography in which ethyl acetate and hexane (1 : 3 by volume) served as the mobile phase. The fluorescent fraction was clear with the naked eye and isolated; the product was recrystallized by CH_2Cl_2 and hexane (1 : 1 by volume) to give a pure green solid portion of **4CF$_3$-Ga** obtained in the yield of 48% (15 mg). ^{1}H NMR (400 MHz, $CDCl_3$): δ = 8.30 (d, J_{H-H} = 4.90 Hz, 2H), 8.13 (d, J_{H-H} = 4.93 Hz, 2H), 7.44 (t, J_{H-H} = 7.53 Hz, 2H, pyridine-H), 6.91 (broad s, 4H, pyridine-H), 6.53 (broad s, 4H, pyridine-H).^{19}F NMR (377 MHz, C_6D_6): δ = −49.21 (s, 6F), −49.31 (s, 6F), −138.78 (m, 6F, *ortho*-F), −150.37 (t, J_{F-F} = 22.93 Hz, 1F, *para*-F), −150.49 (t, J_{F-F} = 22.57 Hz, 2F, *para*-F), −160.87 (m, 2F, *meta*-F), −162.66 (m, 4F, *meta*-F). MS^- (APCI, negative mode) for $C_{41}H_4F_{27}N_4Ga$: m/z = 1133.9255 (calculated), 1133.9182 (observed).

Synthesis of 3CF$_3$-Al

A dry portion of **3I-Al** (40 mg, 33 μmol) and CuI (0.19 g, 1.0 mmol) was dissolved in 5–10 mL DMF after the solution was sparged for 5 min under the argon atmosphere. Then, methyl-2,2-difluoro-2-(fluorosulfonyl) acetate ($FSO_2CF_2CO_2Me$) was added (0.13 mL, 1.0 mmol) into the reaction with the reaction being maintained at 100 °C. The reaction was monitored by TLC, after an ample time of 10 h, the reaction mixture was quenched and separated with water and CH_2Cl_2 (1 : 1 by volume); then, the solution containing the organic phase was

purified by doing a silica gel chromatography in which ethyl acetate and hexane (1 : 1 by volume) constituted the mobile phase. The fluorescent band was clearly identified by inspection and isolated; the non-volatile product was recrystallized using CH_2Cl_2 and hexane (1 : 1) to afford a pure green solid portion of **3CF$_3$-Al** obtained in a yield of 36% (11 mg). ^{1}H NMR (400 MHz, $CDCl_3$): δ = 9.27 (s, 1H), 8.46 (overlapping d, 2H), 8.32 (overlapping d, 2H), 7.32 (unresolved t, 2H, pyridine-H), 6.66 (broad t, 4H, pyridine-H), 5.32 (broad s, 4H, pyridine-H). ^{19}F NMR (377 MHz, $CDCl_3$): δ = −48.54 (q, J = 12.07 Hz, 3F), −50.32 (q, J = 11.77 Hz, 3F), −52.92 (s, 3F), −137.70 (m, 2F, *ortho*-F), −138.15 (m, 4F, *ortho*-F), −152.43 (t, J = 22.28 Hz, 2F, *para*-F), −152.66 (t, J = 21.70 Hz, 1F, *para*-F), −161.51 (m, 2F, *meta*-F), −163.17 (m, 4F, *meta*-F). MS$^-$ (APCI, negative mode) for $C_{40}H_5F_{24}N_4Al$: m/z = 1023.9945 (calculated), 1024.0003 (observed). MS$^+$ (APCI, positive mode) for $C_{40}H_5F_{24}N_4Al$: m/z = 1024.9979 (calculated), 1024.9583 (observed).

Synthesis of 4CF$_3$-Al

A dry portion of **4I-Al** (40 mg, 30 μmol) and CuI (0.23 g, 1.2 mmol) were dissolved in 5–10 mL DMF which was sparged with argon after 5 min. The reagent methyl-2,2-difluoro-2-(fluorosulfonyl) acetate ($FSO_2CF_2CO_2Me$) (0.16 mL, 1.2 mmol) was then added into the reaction. The temperature of the reaction mixture was maintained at 100 °C. The reaction was monitored by TLC, after an ample time of 10 h, the reaction mixture was then quenched and separated with water and CH_2Cl_2 (1 : 1 by volume); then the organic phase was evaporated. The greenish crude product was purified by silica gel chromatography with ethyl acetate and hexane (1 : 2 by volume) as the mobile phase. The fluorescent parts were collected and precipitated/recrystallized by CH_2Cl_2 and hexane (1 : 1 by volume); importantly, a pure green solid **4CF$_3$-Al** was obtained with a yield of 42% (14 mg). ^{1}H NMR (400 MHz, C_6D_6): δ = 8.10 (d, J_{H-H} = 4.89 Hz, 2H), 7.91 (d, J_{H-H} = 4.88 Hz, 2H), 7.36 (s, 1H, pyridine-H), 5.62 (broad s, 2H, pyridine-H), 5.11 (broad s, 2H, pyridine-H).^{19}F NMR (377 MHz, C_6D_6): δ = −49.23 (s, 6F), −49.30 (s, 6F), −138.72 (m, 6F, *ortho*-F), −150.09 (t, J_{F-F} = 21.70 Hz, 1F, *para*-F), −150.30 (t, J_{F-F} = 21.01 Hz, 2F, *para*-F), −160.74 (m, 2F, *meta*-F), −162.55 (m, 4F, *meta*-F). MS$^-$ (APCI, negative mode) for $C_{41}H_4F_{27}N_4Al$: m/z = 1091.9815 (calculated), 1091.9836 (observed). MS$^+$ (APCI, positive mode) for $C_{41}H_4F_{27}N_4Al$: m/z = 1092.9893 (calculated), 1092.9815 (observed).

Crystal data for 3I-Al

Moiety formula: 4($C_{47}H_{15}AlF_{15}I_3N_6$), 3($C_5H_5N$); sum formula: $C_{203}H_{75}Al_4F_{60}I_{12}N_{27}$, M = 5662.63; orthorhombic, space group $P2_12_12_1$ (19), a = 16.5663(1) Å, b = 22.8606(1) Å, c = 26.4461(1) Å, V = 10 015.55(8) Å^3, Z = 2, T = 100 K, D_c = 1.87757 g cm^{-3}, μ (mm^{-1}) = 15.778, data completeness = 1.83/0.99, θ(max) = 74.504, R (reflections) = 0.0463 (19 527), wR_2 (reflections) = 0.1190 (20 347), S = 1.037, Npar = 1421, CCDC 1868043.‡

Crystal data for 3CF$_3$-Ga

Moiety formula: $C_{40}H_7F_{24}GaN_4O$,2(C_5H_5 N); formula: $C_{50}H_{17}F_{24}GaN_6O$, M = 1243.42; monoclinic, space group $P2_1/c$ (14), a = 24.567(7) Å, b = 7.523(2) Å, c = 25.895(7) Å, V = 4695.3 Å^3, Z = 4, T = 200 K, D_c = 1.75746 g cm^{-3}, μ (mm^{-1}) = 0.730, data completeness = 0.957, θ(max) = 25.053, R (reflections) = 0.0754 (5775), wR_2 (reflections) = 0.2048 (7951), S = 0.893, Npar = 728, CCDC 1915746.‡

Conflicts of interest

There are no conflicts to declare.

Acknowledgements

Z. G. acknowledges the support of this research by a grant from the Israel Science Foundation. D. G. C. acknowledges Z. G., the Schulich Faculty of Chemistry, Technion-Israel Institute of Technology, and support from KAIST for facilitating his sabbatical year.

References

1 (*a*) S. Fukuzumi, *et al.*, *Green Chem.*, 2018, **20**, 948–963; (*b*) X. Dai, D. W. Chen, W. Y. Zhou, *et al.*, *Catal. Commun.*, 2018, **17**, 85–89; (*c*) C. M. White and J. P. Zhao, *J. Am. Chem. Soc.*, 2018, **140**, 13988–14009; (*d*) J. Jiang, J.-X. Wang, X.-T. Zhou, *et al.*, *Chem. – Eur. J.*, 2018, **23**, 2666–2674; (*e*) F. Burg, M. Gicquel, S. Breitenlechner, *et al.*, *Angew. Chem., Int. Ed.*, 2018, **57**, 2953–2957; (*f*) G. Li, *et al.*, *Angew. Chem., Int. Ed.*, 2018, **57**, 1251–1255.

2 (*a*) P. Adler, C. J. Teskey, D. Kaiser, M. Holy, H. H. Sitte and N. Maulide, *Nat. Chem.*, 2019, 329–334; (*b*) C. Varlow, D. Szames, K. Dahl, V. Bernard-Gauthier and N. Vasdev, *Chem. Commun.*, 2018, **54**, 11835–11842; (*c*) E. P. Gillis, K. J. Eastman, M. D. Hill, D. J. Donnelly and N. A. Meanwell, *J. Med. Chem.*, 2015, **58**, 8315–8359; (*d*) Q. Shen, Y.-G. Huang, C. Liu, J.-C. Xiao, Q. Y. Chen and Y. Guo, *J. Fluor. Chem.*, 2015, **179**, 14–22.

3 (*a*) V. S. Barata and A. Postigo, *Coord. Chem. Rev.*, 2013, **257**, 3051–3069; (*b*) A. Studer, *Angew. Chem., Int. Ed.*, 2012, **51**, 8950–8958; (*c*) D. A. M. McClinton, *et al.*, *Tetrahedron*, 1992, **48**, 6555–6566.

4 R. W. Taft, *Chem. Rev.*, 1991, **91**, 165–195.

5 (*a*) O. Wagner, J. Thiele, M. Weinhart, L. Mazutis, D. A. Weitz and R. Haag, *Lab Chip*, 2016, **16**, 65–69; (*b*) M. A. Miller and E. M. Sletten, *Org. Lett.*, 2018, **20**, 6850–6854; (*c*) H. Wang, J. J. Hu, X. P. Cai, J. R. Xiao and Y. Y. Cheng, *Polym. Chem.*, 2016, **7**, 2319–2322; (*d*) C.-U. Lee, R. Khalifehzadeh, B. Ratner and A. J. Boydston, *Macromolecules*, 2018, **51**, 1280–1289.

6 (*a*) G. Valero, X. Companyó and R. Rios, *Chem. – Eur. J.*, 2011, **17**, 2018–2037; (*b*) J. A. Ma and D. Cahard, *Chem. Rev.*, 2004, **104**, 6119–6146; (*c*) J. A. Ma and D. Cahard, *Chem. Rev.*, 2008, **108**, 4203–4278.

7 X. Zhan, *et al.*, *Inorg. Chem.*, 2019, **58**, 6184–6198.

8 (*a*) Y. Kobayashi, I. Kumadaki and S. Kuboki, *J. Fluor. Chem.*, 1982, **19**, 517–520; (*b*) J. Leroy, *J. Fluor. Chem.*, 1991, **53**, 61–70; (*c*) K. E. Thomas, L. J. McCormick, *et al.*, *Angew. Chem., Int. Ed.*, 2017, **56**, 10088–10092; (*d*) S. Shimizu, N. Aratani and A. Osuka, *Chem. – Eur. J.*, 2006, **12**, 4909–1918; (*e*) Y. Terazono and D. Dolphin, *J. Org. Chem.*, 2003, **68**, 1892–1900; (*f*) S. Kang, *et al.*, *Chem. – Asian J.*, 2008, **3**, 2065–2074.

9 (*a*) E. T. Kolle, H. Ingar and A. Ghosh, *Inorg. Chem.*, 2008, **47**, 10469–10478; (*b*) E. T. Kolle, C. Jeanet and A. Ghosh, *Inorg. Chem.*, 2011, **50**, 3247–3251.

10 (*a*) A. Mahammed, B. Mondal, A. Rana and Z. Gross, *Chem. Commun.*, 2014, **50**, 2725–2727; (*b*) L. Wagnert, R. Rubin, A. Berg, A. Mahammed, Z. Gross and H. Levanon, *J. Phys. Chem. B*, 2010, **114**, 14303–14308.

11 Q. C. Chen, M. Soll, A. Mizrahi, I. Saltsman, N. Fridman, M. Saphier and Z. Gross, *Angew. Chem., Int. Ed.*, 2018, **57**, 1006–1010.

12 K. Sudhakar, A. Mizrahi, M. Kosa, N. Fridman, B. Tumanskii, M. Saphier and Z. Gross, *Angew. Chem., Int. Ed.*, 2017, **56**, 9837–9841.

13 (*a*) K. Rybicka-Jasinska, W. Q. Shan, K. Zawada, K. M. Kadish and D. Gryko, *J. Am. Chem. Soc.*, 2016, **138**, 15451–15458; (*b*) K. Rybicka-Jasińska and D. Gryko, *Eur. J. Org. Chem.*, 2017, 2104–2107; (*c*) M. Giedyk, K. Goliszewska and D. Gryko, *Chem. Soc. Rev.*, 2015, **44**, 3391–3404.

14 J. Vestfrid, I. Goldberg and Z. Gross, *Inorg. Chem.*, 2014, **53**, 10536–10542.

15 (*a*) N. Miyaura and A. Suzuki, *Chem. Rev.*, 1995, **95**, 2457–2483; (*b*) R. F. Heck and J. P. Nolley, *J. Org. Chem.*, 1972, **37**, 2320–2322; (*c*) D. Milstein and J. K. Stille, *J. Am. Chem. Soc.*, 1978, **100**, 3636–3638; (*d*) A. S. Guram and S. L. Buchwald, *J. Am. Chem. Soc.*, 1994, **116**, 7901–7902; (*e*) F. Paul, J. Patt and J. F. Hartwig, *J. Am. Chem. Soc.*, 1994, **116**, 5969–5970.

16 A. Mahammed and Z. Gross, *Angew. Chem., Int. Ed.*, 2015, **54**, 12370–12373.

17 (*a*) X. P. Bao, *et al.*, *Org. Lett.*, 2017, **19**, 5780–5782; (*b*) Y. J. Yang, *et al.*, *ACS Appl. Mater. Interfaces*, 2017, **9**, 30958–30963; (*c*) X. T. Ma and S. K. Tian, *Adv. Synth. Catal.*, 2013, **355**, 337–340; (*d*) R. K. Chinnagolla, *et al.*, *Chem. Commun.*, 2013, **49**, 3146–3148.

18 (*a*) K. Ohkubo, A. Fujimoto and S. Fukuzumi, *J. Am. Chem. Soc.*, 2013, **135**, 5368–5371; (*b*) K. Ohkubo, T. Kobayashi and S. Fukuzumi, *Angew. Chem., Int. Ed.*, 2011, **50**, 8652–8655; (*c*) H. Kotani, K. Ohkubo and S. Fukuzumi, *J. Am. Chem. Soc.*, 2004, **126**, 15999–16006; (*d*) K. Ohkubo, K. Mizushima, R. Iwata and S. Fukuzumi, *Chem. Sci.*, 2011, **2**, 715–722; (*e*) S. Fukuzumi and K. Ohkubo, *Org. Biomol. Chem.*, 2014, **12**, 6059–6071.

19 N. V. Klassen, D. Marchington and H. C. E. McGowan, *Anal. Chem.*, 1994, **66**, 2921–2925.